Scripta Materialia 222 (2023) 115027

Contents lists available at ScienceDirect

Scripta Materialia

journal homepage: www.journals.elsevier.com/scripta-materialia

A simple method enabling efficient quantitative analysis of the Portevin–Le Chatelier band characteristics

Jianbin Xu [a,b,*], Lei Liu [c], Odd Sture Hopperstad [b], Bjørn Holmedal [a], Tomáš Mánik [a], Knut Marthinsen [a]

[a] Department of Materials Science and Engineering, Norwegian University of Science and Technology (NTNU), Sem Sælands vei 14, Trondheim 7491, Norway
[b] Centre for Advanced Structural Analysis (CASA), Department of Structural Engineering, Norwegian University of Science and Technology (NTNU), Richard Birkelands vei 1a, Trondheim 7491, Norway
[c] Department of Mechanical Engineering, Eindhoven University of Technology, 5600 MB Eindhoven, the Netherlands

ARTICLE INFO

Keywords:
Portevin–Le Chatelier effect
Dynamic strain aging
Spatio-temporal behaviour
Quantitative analysis

ABSTRACT

Localized deformation bands are often observed in materials exhibiting the Portevin–Le Chatelier (PLC) effect. However, efficient quantitative analysis of PLC bands remains challenging. A novel method is thus proposed in this work, where a multi-strain-jump function is introduced to capture the experimentally obtained staircase-like strain profile from digital image correlation (DIC). This approach is simple to implement and allows for: (i) automatically extracting the band strain throughout the test, which can be used to further evaluate the band velocity, and (ii) linking band characteristics with the corresponding local material properties. The efficiency of the method is demonstrated by analysing the band characteristics for different strain rates and temperatures. The results reveal that the relative band velocity is proportional to the work hardening rate, i.e., $v_b/v_g \propto \Theta$, for the continuously propagating type A bands.

The Portevin–Le Chatelier (PLC) effect is associated with repeated nucleation of deformation bands in many alloys, *e.g.*, mild steel [1], Ni based superalloys [2], and Al-Mg alloys [3]. The macroscopic manifestation of the PLC effect originates from the microscopic dynamic strain ageing (DSA) process [4]. In a certain range of strain rate and temperature, the prevailing solute diffusion strongly influences the dislocation motion, resulting in an abnormal negative strain rate sensitivity (nSRS) of the material and thus the instabilities during the deformation [5,6]. Based on different spatial-temporal patterns, the PLC bands are usually classified into three types: continuous (type A), semi-continuous (type B), and discontinuous (type C) bands [7]. Great efforts have been made to investigate the PLC band behaviour. However, up to now most existing studies qualitatively relate the band characteristics to the overall material properties [3,5,8], *e.g.*, global strain, which contradicts the nature of the highly localized PLC deformation. This motivates the present study where a direct connection between the band behaviour and the material's intrinsic properties is established.

Two band characteristics, *i.e.*, band strain ε_b and band velocity v_b, are often used to describe the PLC band behaviour. Conventionally, the band strain is calculated manually from the strain profile [9–11] and the band velocity is estimated from the slope of PLC spatial-temporal patterns [12]. However, this method often suffers from low accuracy and efficiency, and thus may not provide enough high-quality data points for subsequent quantitative analysis. Moreover, such a method becomes even nonapplicable to the type C band due to its spatially disordered feature. To address these challenges, a novel method that enables efficient quantitative analysis of the band strain and velocity is firstly proposed. With the developed method, quantitative analysis of experimental results obtained at different strain rates and temperatures is demonstrated.

Uniaxial tension tests were conducted for the commercial aluminium alloy AA5182-O. A constant crosshead velocity of either 6 mm s^{-1} or 0.06 mm s^{-1} was applied using a servo-hydraulic 100 kN MTS testing machine at 298 K, which yielded nominal strain rates of $10^{-1}s^{-1}$ and 10^{-3} s^{-1}, respectively. Tests at elevated temperatures, *i.e.*, 325 K and 378 K, were also performed at $10^{-1}s^{-1}$. Full-field strain measurements were performed using digital image correlation (DIC). A high-speed CCD camera was utilized with sampling rates equal to 5 Hz and 200 Hz for the

* Corresponding author at: Centre for Advanced Structural Analysis (CASA), Department of Structural Engineering, Norwegian University of Science and Technology (NTNU), Richard Birkelands vei 1a, NO-7491 Trondheim, Norway
E-mail address: jianbin.xu@ntnu.no (J. Xu).

https://doi.org/10.1016/j.scriptamat.2022.115027
Received 14 July 2022; Received in revised form 29 August 2022; Accepted 29 August 2022
Available online 6 September 2022

slow and fast tests, respectively. A 60 mm virtual extensometer, which is discretized into 200 evenly distributed data grid points, was applied to record the local axial logarithmic strain ε_{xx} at every material point on the surface of the gauge section as a function of the global engineering strain, see Fig. 1a. More details can be found in our previous work [4].

The engineering stress-strain curves in Fig. 1b show a nSRS, *i.e.*, the stress level decreases with increasing strain rate at 298 K. The response curve at a low strain rate demonstrates more pronounced oscillations than the one at a high strain rate, which is known to strongly correlate with the band nucleation and propagation [13]. Fig. 1c shows the spatio-temporal patterns, in which the band strain rate is defined by the strain increment between two successive frames: $\dot{\varepsilon}_{xx} \approx (\varepsilon_{xx}(t_2) - \varepsilon_{xx}(t_1))/(t_2 - t_1)$ [13]. At $10^{-1}s^{-1}$, the band propagates continuously and is usually referred to as type A band, in which long segments of inclined lines are observed. The band velocity can be roughly estimated from the slope of these lines, see the red dashed line. At $10^{-3}s^{-1}$, the band motion becomes more discontinuous compared to that at high strain rate.

In Fig. 2a, the strain profiles measured at all time instants are plotted throughout the test. The strain is nonuniformly accumulated. After the onset of the PLC instability, a strain increment, *i.e.*, the band strain, remains at the place where the PLC band front has swept by. Localized necking and immobilization of the PLC band occur nearby the position of $x = 20$ mm. The band strain is usually manually obtained by measuring the height of the strain profile, see the inserted figure. A vertical line at $x = 42$ mm is drawn as an example, and the black arrows indicate all strain increments across this chosen position. However, it is not always easy to measure the band strain in this way. In the region x ∈ [35 mm, 40 mm], the band strain is not readily defined. Moreover, this approach is impossible to perform for tests at $10^{-3}s^{-1}$ since the band strain is accumulated in a disordered manner.

To avoid these issues, an alternative method for measuring the band strain is proposed by directly plotting the staircase-like strain history of a specific position, see Fig. 2b. Each time a PLC band front hits or passes the selected position, a strain burst will be generated, leading to a series of jumps in the strain history. The height of each jump indicates the magnitude of the band strain, as denoted in the inserted figure. The corresponding engineering strain of the jump represents the moment when this local strain jump event occurs. Since the strain history profile at either $10^{-1}s^{-1}$ or $10^{-3}s^{-1}$ follows a similar staircase-like shape, the proposed method is applicable to both continuous and discontinuous

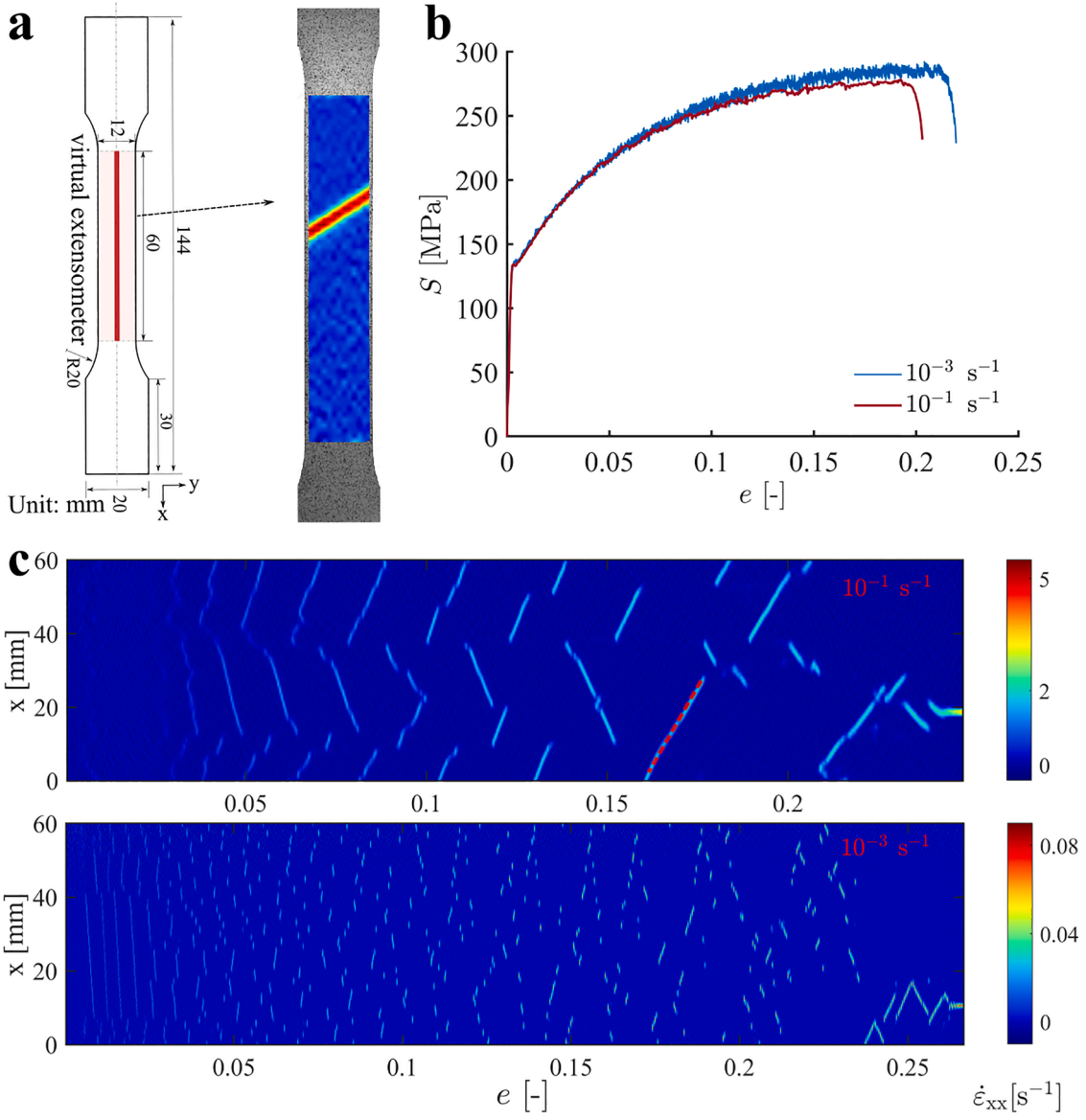

Fig. 1. (a) Geometry of the uniaxial tension specimen with thickness 1.2 mm, (b) engineering stress-strain curves at 298 K, and (c) time variation of the local strain rate along the centreline of the gauge length at strain rate of 10^{-1} s^{-1} and 10^{-3} s^{-1}.

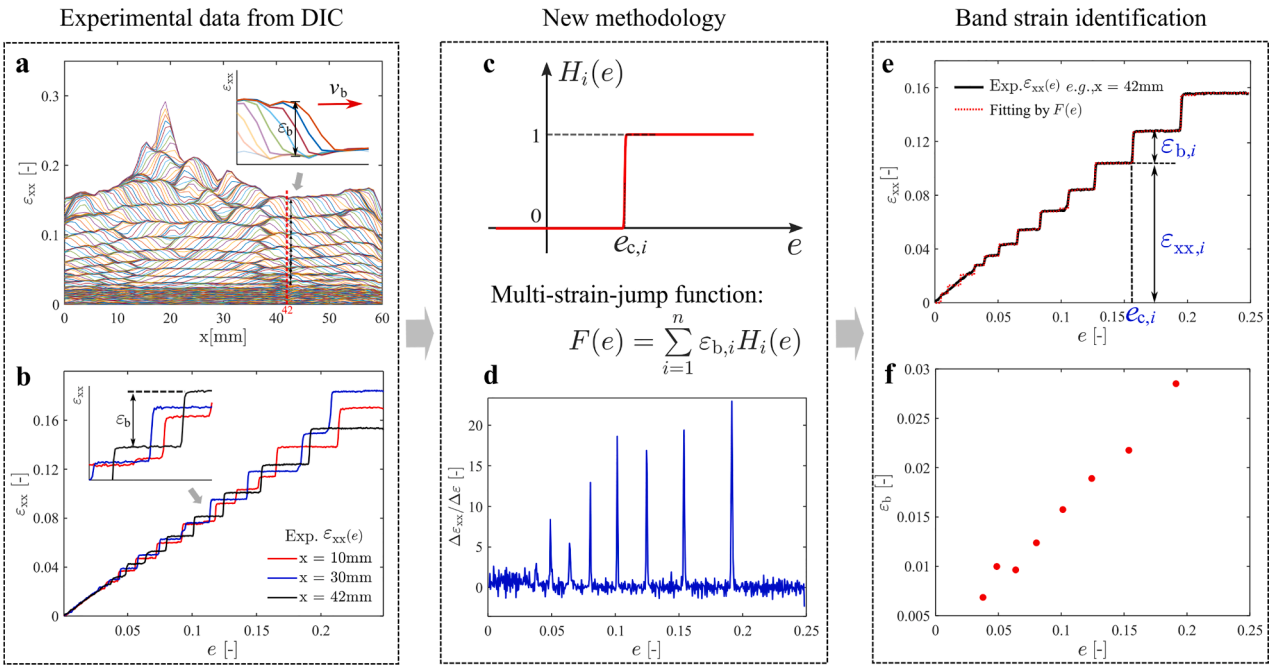

Fig. 2. Experimental results from DIC measurements for test at 10^{-1} s^{-1}: (a) strain accumulation along the virtual gauge, and (b) strain histories at three positions. New methodology: (c) schematic illustration of the single strain jump function, and (d) numerical derivative of the strain history data at $x = 42$ mm. Band strain identification: (e) fitted strain history curve and automatically obtained $e_{c,i}$ $\varepsilon_{b,i}$ and $\varepsilon_{xx,i}(i = 1, 2, 3, \ldots)$, and (f) band strain at $x = 42$ mm.

spatio-temporal patterns. Such a staircase-like shape of the strain history data can be identified using the following multi-strain-jump function

$$F(e)=\sum_{i=1}^{n}\varepsilon_{b,i}H_i(e) \tag{1}$$

where, e denotes the global engineering strain,n the total number of strain jumps, $\varepsilon_{b,i}$ the step height around each strain jump, which is resolved by a Heaviside step function centered at the strain jump position $e_{c,i}$(see Fig. 2c)

$$H_i(e)=\begin{cases}0, & e\leqslant e_{c,i}\\ 1, & e>e_{c,i}\end{cases} \tag{2}$$

For convenience of implementation, a smooth regularized form of $H_i(e)$ is applied, namely, $H_i^r(e)=\frac{1}{2}+\frac{1}{2}\tanh\frac{1}{\delta}(e-e_{c,i})$, where the parameter δ indicates the sharpness at the strain jump and is here set equal to 0.01. Other regularized forms of $H_i(e)$are also possible and the specific choice does not affect the use of Eq. (1), provided the corresponding sharpness parameter is sufficiently small. In addition, the value of n required in Eq. (1) is generally unknown beforehand, but can be estimated by numerically differentiating the strain history data (see Fig. 2b), leading to a set of local peaks reflecting the dominating strain jumps (see Fig. 2d). The positions of these local peaks also provide the initial guess for identifying the values of $e_{c,i}$. To capture all important strain jumps, the adopted value of n is suggested to be larger than its estimate and set as 30 in this work. With the proposed function $F(e)$ and the experimental data set $\varepsilon_{xx}(e)$, a least square minimization problem can be formulated as,

$$\min_{\varepsilon_{b,i},\ e_{c,i}}\sum_{k=1}^{m}\left(F(e_k)-\varepsilon_{xx}(e_k)\right)^2 \tag{3}$$

where, $\varepsilon_{b,i}$ and $e_{c,i}$ are the desired parameters, and m is the number of discrete experimental data points. One example of the above minimization is given in Fig. 2e, showing that the staircase-like strain history profile can be captured well by the proposed multi-strain-jump function. Note that some spurious strain jumps appear due to the high number setting of n, which are however negligible compared to the dominating strain jumps and do not affect the subsequent analysis. The magnitude of the strain bursts $\varepsilon_{b,i}$ $(i = 1, 2, 3, \ldots)$ and the corresponding engineering strains $e_{c,i}$ are automatically obtained and recorded in Fig. 2f. Moreover, the current method gives the local accumulated strains $\varepsilon_{xx,i}$ before the strain bursts, which enables investigation of the correlation between the plastic instability and the local microstructure evolution. The MATLAB implementation of the currently proposed method can be found in the supplementary material.

With the method described above, congregated data for 200 positions equally distributed along the gauge length are obtained. Fig. 3a shows that the band strain increases as the deformation proceeds. Besides, it is clearly seen that the band strain also increases with the externally applied strain rate. For materials that exhibit the PLC effect, the imposed deformation is almost solely achieved by a single "propagating" or "hopping" band. The band strain ε_b and band velocity v_b are highly correlated and given by Rizzi and Hähner [14],

$$v_b \approx v_g \,/\, \varepsilon_b \tag{4}$$

where, v_g is the elongation speed measured by the virtual extensometer. The value of v_g can be obtained from the DIC analysis, which is 4.358 mm s^{-1} at $10^{-1}s^{-1}$ and 0.043 mm s^{-1} at $10^{-3}s^{-1}$, respectively. The band velocities can then be easily obtained by Eq. (4). It should be stated that the average band velocity v_b, as defined in Fig. 1c, might not be a well-defined quantity for discontinuous bands. However, it could still serve as an indicator for describing the average band kinematics. Moreover, the band velocity defined by Eq. (4) provides a unified description of the band behaviour and renders it possible to evaluate the band kinematics even for the discontinuous band scenario. As we know, the value of the band velocity strongly depends on the externally applied strain rate. Therefore, the relative band velocity, v_b/v_g, is utilized instead for a direct comparison of the band kinematics at different strain rates. Fig. 3b shows that the relative band velocity decreases asymptotically towards zero in both tests. Interestingly, the relative band velocity is lower at $10^{-1}s^{-1}$ than the one at $10^{-3}s^{-1}$, which indicates that the applied strain rate is not the only decisive factor that influences the band kinematics.

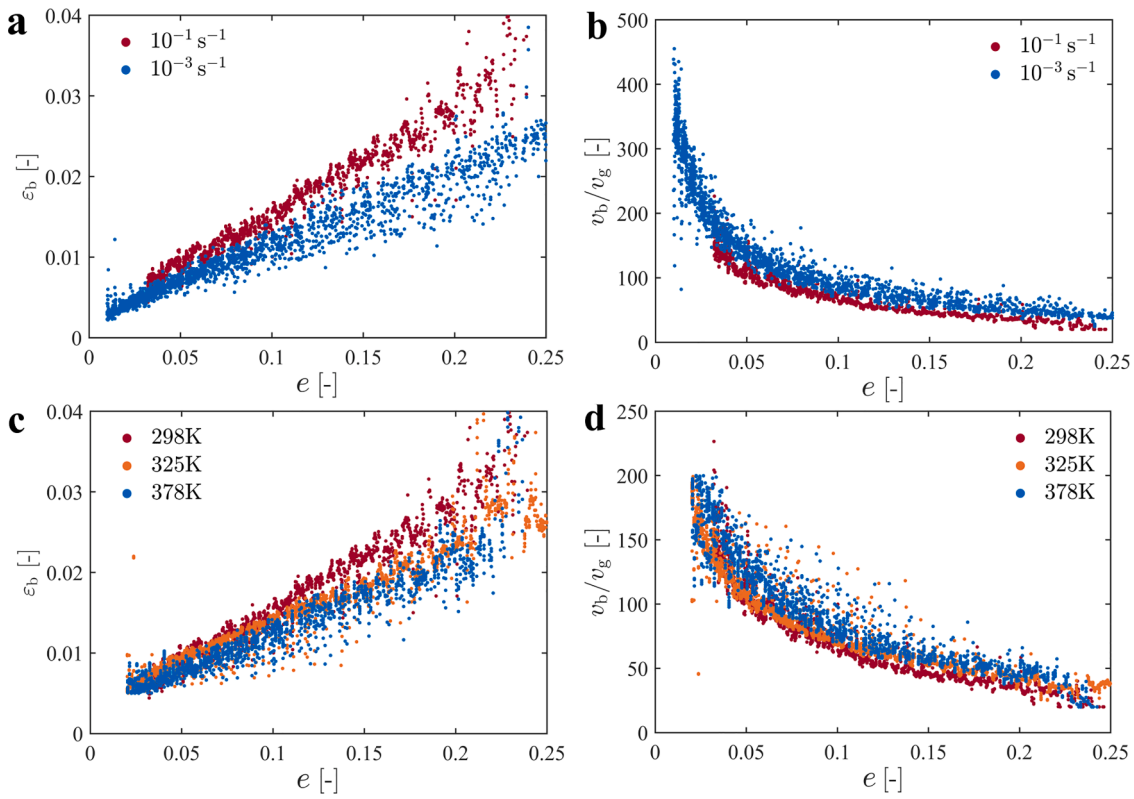

Fig. 3. Band characteristics vs engineering strain at different strain rates and temperatures: (a, c) band strain ε_b and (b, d) relative band velocity v_b/v_g. The figures congregate data for all 200 cross sections.

All the above discussions are based on tests at a given temperature. However, it is well known that the temperature plays important roles as well, not only in the thermally activated dislocation movement, but also on the diffusion-related DSA process [4]. Fig. 3c and d show the band strain ε_b and the relative band velocity v_b/v_g vs global engineering strain e at temperatures 298 K, 325 K and 378 K and strain rate 10^{-1}s^{-1}. Although temperature does not change the main band characteristics, it influences the values of both ε_b and v_b. It is found that the band strain decreases with increasing temperatures, while the relative band velocity increases with increasing temperatures. All factors that influence the band characteristics are summarized in Table 1.

As shown above, the band characteristics can be efficiently obtained with the proposed method. However, one question still remains open with the above analysis: is it appropriate to build a direct connection between the band characteristics and the global deformation? Fortunately, the current method offers the possibility of linking the band characteristics and the corresponding local work hardening properties. The local work hardening rate Θ can be estimated by the following steps:

- firstly, the experimental true stress–strain curve is fitted by an extended Voce hardening rule using four additive terms, *i.e.*, $\sigma(\varepsilon_p) = \sigma_0 + \sum_{i=1}^{4} Q_i(1 - \exp(-C_i\varepsilon_p))$, where σ_0, Q_i and C_i are fitting constants and ε_p is the plastic strain;
- secondly, once the true stress–strain curve has been fitted, the work hardening of the materials can be calculated as $\Theta(\varepsilon_p) = d\sigma/d\varepsilon_p = \sum_{i=1}^{4} Q_i C_i \exp(-C_i\varepsilon_p)$;
- thirdly, the current method gives the as-built local strain accumulation $\varepsilon_{xx,i}$ prior to any PLC deformation event, and the corresponding local work hardening rate is given by $\Theta_i = \Theta(\varepsilon_{xx,i})$, where $\varepsilon_{xx,i}$ is assumed approximately equal to the local plastic strain.

Table 1
Factors that influence the PLC band characteristics.

	Strain	Strain rate	Temperature	Work hardening
Band strain ε_b	↑	↑	↓	↓
Band velocity v_b.	↓	↑	↑	↑

↑, positive correlation; ↓, negative correlation.

Fig. 4a shows the variation of the relative band velocity with the normalized work hardening rate at different strain rates, where Young's modulus E is given by 71.9 GPa (298 K), 69.6 GPa (325 K) and 66.7 GPa (378 K). The relative band velocity is approximately proportional to the work hardening rate, *i.e.*, $v_b/v_g \propto \Theta$, for the type A band at 10^{-1}s^{-1}. Similar findings have recently been reported based on a lower-scale study [15], and a detailed theoretical analysis can be found in a currently submitted work [16]. At 10^{-3}s^{-1}, a nearly linear increase is seen for low work hardening rates as well, however, v_b/v_g increases very rapidly for higher work hardening rates. Similar results at different temperatures are obtained in Fig. 4b, and deviations from linearity are found for higher work hardening rates in the test at 378 K. Although not shown here, a further experimental check of the spatio-temporal behaviour of the PLC band at elevated temperatures has been conducted. It is found that the PLC bands also become discontinuous at 378 K. The reason for this may stem from different collective dislocation dynamics of the hopping band at the low strain rate or high temperatures. More work is needed to disclose the underlying mechanisms for the different band characteristics.

In summary, a simple method is introduced to automatically obtain the band strain and the band velocity for both spatially ordered and disordered PLC bands. Moreover, a direct link between the band characteristics and the corresponding accumulated local strain is established. The results reveal that the relative band velocity is proportional to the work hardening rate, *i.e.*, $v_b/v_g \propto \Theta$, for the continuously

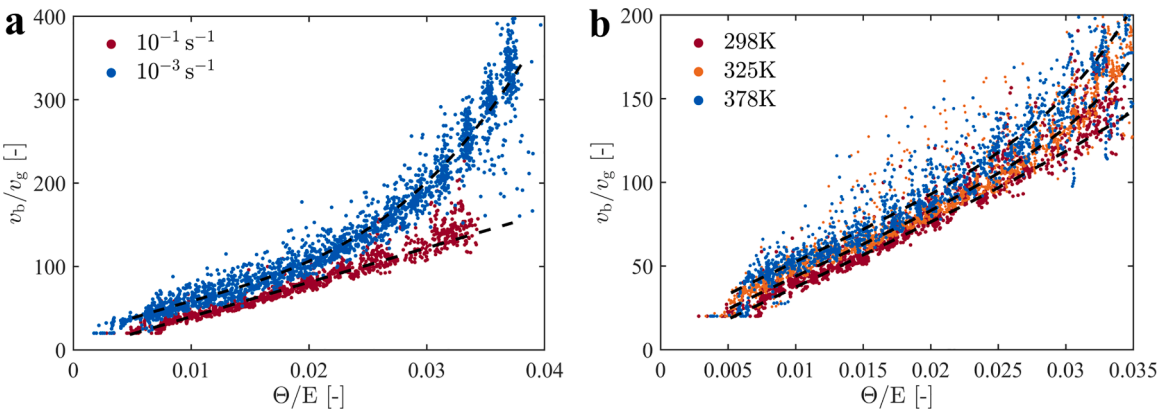

Fig. 4. Relative band velocity v_b/v_g. vs normalized work hardening rate Θ/E at: (a) different strain rates, 298 K; (b) different temperatures, 10^{-1} s^{-1}. The work hardening rate is calculated based on the local strain accumulation, *i.e.*, $\Theta_i = \Theta(\varepsilon_{xx,i})$. The dashed lines denotes the average trend of the scattered data.

propagating type A band. This new approach may open up for efficient quantitative analysis of the band characteristics and can be extended to any material that exhibits the PLC effect.

Declaration of Competing Interest

The authors declare that they have no known competing financial interests or personal relationships that could have appeared to influence the work reported in this paper.

Acknowledgment

This research was conducted at the Centre for Advanced Structural Analysis (CASA), funded by the Research Council of Norway (grant number 237885) and several public and company partners.

Supplementary materials

Supplementary material associated with this article can be found, in the online version, at doi:10.1016/j.scriptamat.2022.115027.

Reference

[1] P. McCormick, The Portevin-Le Chatelier effect in a pressurized low carbon steel, Acta Metall. 21 (7) (1973) 873–878.
[2] C. Cui, R. Zhang, Y. Zhou, X. Sun, Portevin-Le Châtelier effect in wrought Ni-based superalloys: experiments and mechanisms, J. Mater. Sci. Technol. 51 (2020) 16–31.
[3] O. Hopperstad, T. Børvik, T. Berstad, O. Lademo, A. Benallal, A numerical study on the influence of the Portevin–Le Chatelier effect on necking in an aluminium alloy, Model. Simul. Mater. Sci. Eng. 15 (7) (2007) 747.
[4] J. Xu, B. Holmedal, O.S. Hopperstad, T. Mánik, K. Marthinsen, Dynamic strain ageing in an AlMg alloy at different strain rates and temperatures: experiments and constitutive modelling, Int. J. Plast. 151 (2022), 103215.
[5] A. Benallal, T. Berstad, T. Børvik, O.S. Hopperstad, I. Koutiri, R.N. de Codes, An experimental and numerical investigation of the behaviour of AA5083 aluminium alloy in presence of the Portevin–Le Chatelier effect, Int. J. Plast. 24 (10) (2008) 1916–1945.
[6] A. Benallal, T. Berstad, T. Børvik, O.S. Hopperstad, R. Nogueira de Codes, Effects of strain rate on the characteristics of PLC deformation bands for AA5083-H116 aluminium alloy, Philos. Mag. 88 (28–29) (2008) 3311–3338.
[7] M. Lebyodkin, L. Dunin-Barkowskii, Y. Brechet, Y. Estrin, L. Kubin, Spatio-temporal dynamics of the Portevin–Le Chatelier effect: experiment and modelling, Acta Mater. 48 (10) (2000) 2529–2541.
[8] D. Yuzbekova, A. Mogucheva, D. Zhemchuzhnikova, T. Lebedkina, M. Lebyodkin, R. Kaibyshev, Effect of microstructure on continuous propagation of the Portevin–Le Chatelier deformation bands, Int. J. Plast. 96 (2017) 210–226.
[9] B. Reyne, P.Y. Manach, N. Moes, Macroscopic consequences of Piobert–Lüders and Portevin–Le Chatelier bands during tensile deformation in Al-Mg alloys, Mater. Sci. Eng. A 746 (2019) 187–196.
[10] J. Kang, R.K. Mishra, D.S. Wilkinson, O.S. Hopperstad, Effect of Mg content on Portevin–Le Chatelier band strain in Al–Mg sheet alloys, Philos. Mag. Lett. 92 (11) (2012) 647–655.
[11] Y. Cai, S. Yang, S. Fu, D. Zhang, Q. Zhang, Investigation of Portevin–Le Chatelier band strain and elastic shrinkage in Al-based alloys associated with Mg contents, J. Mater. Sci. Technol. 33 (6) (2017) 580–586.
[12] D. Zhemchuzhnikova. Influence of the Extreme Grain Size Reduction on Plastic Deformation Instability in an AlMg and AlMgScZr Alloys, Université de Lorraine, 2018.
[13] B. Klusemann, G. Fischer, T. Böhlke, B. Svendsen, Thermomechanical characterization of Portevin–Le Châtelier bands in AlMg3 (AA5754) and modeling based on a modified Estrin–McCormick approach, Int. J. Plast. 67 (2015) 192–216.
[14] E. Rizzi, P. Hähner, On the Portevin–Le Chatelier effect: theoretical modeling and numerical results, Int. J. Plast. 20 (1) (2004) 121–165.
[15] T. Mäkinen, P. Karppinen, M. Ovaska, L. Laurson, M.J. Alava, Propagating bands of plastic deformation in a metal alloy as critical avalanches, Sci. Adv. 6 (41) (2020) eabc7350.
[16] J. Xu, O.S. Hopperstad, B. Holmedal, T. Mánik, K. Marthinsen, On the spatio-temporal characteristics of the Portevin-Le Chatelier effect in aluminium alloy AA5182: an experimental and numerical study, Submitted.